AGU PUBLICATIONS

JGR

Journal of Geophysical Research: Atmospheres

RESEARCH ARTICLE
10.1002/2013JD020453

Special Section:
Suomi NPP Calibration and Validation Scientific Results

Active fires from the Suomi NPP Visible Infrared Imaging Radiometer Suite: Product status and first evaluation results

Ivan Csiszar[1], Wilfrid Schroeder[2], Louis Giglio[2], Evan Ellicott[2], Krishna P. Vadrevu[2], Christopher O. Justice[2], and Brad Wind[3]

[1]NOAA/NESDIS Center for Satellite Applications and Research, College Park, Maryland, USA, [2]Department of Geographical Sciences, University of Maryland, College Park, Maryland, USA, [3]Enterprise Information Solutions, Inc., Columbia, Maryland, USA

Key Points:
- The VIIRS sensor demonstrated good performance for active fire detection
- VIIRS fire detections are consistent with coincident MODIS detections
- The product provides reliable information for near real-time monitoring

Correspondence to:
Ivan Csiszar,
ivan.csiszar@noaa.gov

Citation:
Csiszar, I., W. Schroeder, L. Giglio, E. Ellicott, K. P. Vadrevu, C. O. Justice, and B. Wind (2014), Active fires from the Suomi NPP Visible Infrared Imaging Radiometer Suite: Product status and first evaluation results, *J. Geophys. Res. Atmos.*, *119*, doi:10.1002/2013JD020453.

Received 2 JUL 2013
Accepted 14 DEC 2013
Accepted article online 18 DEC 2013

Abstract The Visible Infrared Imaging Radiometer Suite (VIIRS) sensor on the Suomi National Polar-orbiting Partnership (S-NPP) satellite incorporates fire-sensitive channels, including a dual-gain high-saturation temperature 4 μm channel, enabling active fire detection and characterization. The active fire product, based on the 750 m moderate resolution "M" bands of VIIRS, is one of the standard operational products generated by the Interface Data Processing Segment of the S-NPP ground system. The product builds on an earlier "Collection 4" version of the algorithm used for processing Moderate Resolution Imaging Spectroradiometer (MODIS) data. Following postlaunch quality assessments and corrections in the input VIIRS Sensor Data Record data processing, an initial low detection bias was removed and the product achieved Beta quality in April 2012. Daily spurious detections along-scan lines were also significantly reduced as a result of further processing improvements in October 2012. Direct product comparison with MODIS over 4 months of data in 2013 has shown that VIIRS produces approximately 26% more detections than MODIS within the central 3 pixel VIIRS aggregation zone of approximately ±31° scan angle range and 70% more detections outside of that zone, mainly as a result of the superior VIIRS scanning and sampling characteristics. Further development is in progress to ensure high-quality VIIRS fire products that continue the MODIS data record and better serve the user community by delivering a full image classification product and fire radiative power retrievals. Research is also underway to take advantage of the radiometric signal from the 375 m VIIRS imager "I" bands.

1. Introduction

Active fire data from spaceborne sensors have been available since the 1980s [*Ichoku et al*., 2012; *Matson and Holben*, 1987; *Setzer and Pereira*, 1991]. The increased thermal signal of active fires in the 4 μm channel, together with radiometric measurements in the longwave and shortwave channels, enables the detection of thermal anomalies from moderate to coarse spatial resolution sensors [*Dozier*, 1981; *Robinson*, 1991] for a wide range of environmental and observing conditions [*Giglio et al*., 1999]. The series of U.S. polar orbiter environmental satellites provided a crucial contribution to the international suite of sensors flown by various space agencies on both polar and geostationary platforms [*Justice et al*., 2013a]. On the National Oceanic and Atmospheric Administration's (NOAA) polar orbiters, the 1 km advanced very high resolution radiometer (AVHRR) sensor has been used worldwide for operational fire monitoring and for research purposes since the early 1990s [*Justice and Tucker*, 2009], with different algorithms using the signal from the fire's thermal emission in the 3.7 μm channel as the main driver for active fire detection [*Giglio et al*., 1999; *Li et al*., 2000; *Lasaponara et al*., 2003]. A number of operational fire monitoring systems around the world have been using AVHRR as one of the primary sensors. Examples include the NOAA Hazard Mapping System (http://www.osdpd.noaa.gov/ml/land/hms.html), the Brazilian National Institute for Space Research operational fire monitoring system (http://www.inpe.br/queimadas/), the South African Advanced Fire Information System (http://www.afis.co.za/), and the Canadian Wildland Fire Information System (http://cwfis.cfs.nrcan.gc.ca/en_CA/background/dsm/fm3). Efforts also have been made to use nighttime visible data from the Operational Linescan Imager (OLS) sensor on the Defense Meteorological Satellite Program satellites to identify fires [*Elvidge et al*., 2001].

Routine global active fire observations are now available for over a decade from the 1 km resolution Moderate Resolution Imaging Spectroradiometer (MODIS) instruments aboard the NASA Earth Observing System (EOS)

Terra and Aqua satellites with spectral bands specifically configured to detect fires [*Justice et al*., 2002]. MODIS represented a major advance in fire observations, allowing the production of 1 km global fire detection product with fewer saturated pixels, and improved geolocation and orbit stability compared to its predecessors [*Justice et al*., 2011a]. The retrieval of fire radiative power (FRP) created new possibilities for direct application of the data toward biomass burning emissions and air quality studies [*Kaufman et al*., 1998; *Wooster et al*., 2003; *Ichoku and Kaufman*, 2005]. A major effort was designed to comprehensively assess and validate the quality of the data produced, which in turn allowed the continuous refinement of the *Fire and Thermal Anomalies* algorithm applied to MODIS Terra and Aqua data (MOD14 and MYD14) [*Giglio et al*., 2003]. As a result, the product has achieved Stage 3 validation maturity as defined by the NASA Earth Observing System (http://landval.gsfc.nasa.gov/). The maturity of the MODIS fire product is also evidenced by the large number of citations and data applications found in the literature.

The new generation U.S. operational medium resolution imager, the Visible Infrared Imaging Radiometer Suite (VIIRS) [*Cao et al*., 2013a], provides radiometric measurements in the midwave infrared around 4 μm that, similar to heritage sensors, offer useful information for the detection and characterization of active fires during both the day and nighttime parts of the satellite orbit. The sampling and radiometric features of VIIRS hold the potential for the best quality global operational fire monitoring to date. An additional day-night band (DNB) (0.5–0.9 μm) detects the visible and near-infrared portion of the fire thermal emission signal, which can be detected only at nighttime due to the overwhelming signal from reflected solar radiation during the day. This is a similar concept to the use of the heritage OLS product, but the VIIRS spatial resolution and radiometric quality are much better. Discussion of nighttime DNB detection capabilities can be found in *Hillger et al*. [2013]. Other VIIRS bands in the shortwave part of the spectrum can also be used for the detection and characterization of hot sources [*Elvidge et al*., 2013].

The first VIIRS sensor onboard the Suomi National Polar-orbiting Partnership (S-NPP) satellite was launched on 28 October 2011. Subsequent operational VIIRS sensors are planned on the Joint Polar Satellite System (JPSS) J1 and J2 satellites [*Justice et al*., 2011b]. This paper focuses on the VIIRS day and nighttime active fire detection capabilities based primarily on the midwave and longwave infrared channel data, continuing the AVHRR and especially MODIS heritage approach. It describes product development, validation, and user readiness activities to serve a worldwide user community of active fire information.

2. VIIRS Sensor Characteristics for Fire Monitoring

The VIIRS sensor was designed to operate with a specific pixel aggregation scheme that impacts fire detection through the resulting spatial sampling, and to some extent, also the radiometric signal. Actual radiometric measurements are made by native resolution pixels, having approximate pixel sizes of 750 m × 250 m at nadir for moderate resolution M bands (for "imagery" resolution I bands the pixel lateral dimensions are half of those of the M bands). Between nadir view and a scan angle of 31.58°, three native resolution pixels are aggregated into a single nominal pixel. Between 31.58° and 44.6°, two native resolution pixels are aggregated, and beyond the 44.6° scan angle single native resolution pixels constitute a nominal pixel. As a result, the along-scan growth of pixel size is significantly reduced compared to sensors without a similar aggregation scheme, such as MODIS or AVHRR [*Wolfe et al*., 2013]. While for the latter sensors fire detection capabilities significantly degrade for off-nadir views; the degradation for VIIRS is far smaller. However, as a discontinuity occurs in the VIIRS pixel size at the aggregation switchover angles, the lower limits for detectable fire temperature and area also change more significantly at those angles.

The primary VIIRS data input for active fire detection and characterization is the moderate resolution M13 channel, which encompasses the spectral region between 3.973 μm and 4.128 μm. M13 is a dynamically controlled dual-gain band, which was specifically designed for hot target detection and characterization, with nominal saturation temperatures of 343 K and 634 K and at high and low gain settings, respectively. The M13 data are aggregated on the ground, and native resolution unaggregated data are available to the VIIRS science teams.

The secondary band in the VIIRS fire detection algorithm used to characterize background thermal conditions is M15 at 10.263–11.263 μm. This is a single-gain band, which is subject to the same pixel aggregation scheme described above. However, contrary to the M13 channel, the M15 data are aggregated onboard the spacecraft before being relayed to the ground stations; therefore, native resolution, unaggregated data are unavailable. A challenge for fire detection and characterization is the relatively low M15 saturation threshold (363 K), which may be reached in the native resolution pixels for moderate-to-large fires. As there is currently

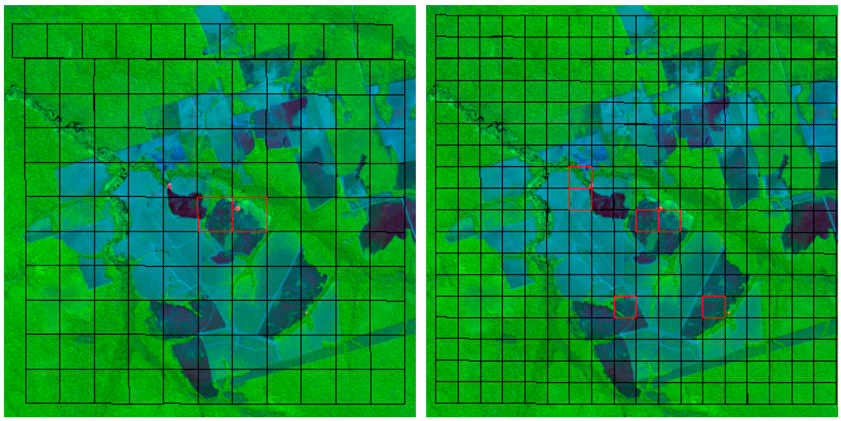

Figure 1. Example of observed (left) MODIS and expected (right) VIIRS detection performance demonstrated using an ASTER scene acquired in the Amazon (11.7°S, 56.6°W) on 7 August 2004 at 14:05 UTC. The VIIRS detections are based on simulated radiances. Red areas on the ASTER scene represent locations of fires detected by ASTER. The red contours are pixels flagged as "fire" by MODIS and simulated VIIRS, respectively.

no flag that indicates the presence of saturated, preaggregated native resolution pixels, the M15 radiance values for some aggregated fire pixels may consequently be spurious. Our prelaunch data analyses have shown that while the fraction of such mixed saturated and unsaturated M15 fire pixels is up to ~3% globally, this is neither expected to result in any measurable degradation of the fire detection nor of the single-band FRP retrieval as it is based on the primary 4 μm channel data [*Schroeder et al*., 2010; *Wooster et al*., 2003]. However, this data artifact is expected to impact the retrieval of fire temperature/area or flaming/smoldering ratios based on bispectral methods using the midwave and longwave infrared channels for a range of fire characteristics and observing conditions [*Giglio and Justice*, 2003]. In addition to saturation issues, fire property retrievals are also impacted by atmospheric and further instrument effects [*Giglio and Kendall*, 2001]. For the key M13 and M15 bands, the prelaunch ground band-to-band registration test result, under thermal vacuum for nominal performance plateau, is 0.86 [*Cao et al*., 2013a]. This is estimated to have a minimal impact on fire detection but would impact area/temperature retrievals, with additional sensitivity to VIIRS pixel spatial response and aggregation effects [*Shephard and Kennelly*, 2003].

As the primary driver of lower fire detection limit for any given fire temperature is pixel size (assuming unsaturated measurements), the nominally 750 m × 750 m nadir resolution VIIRS is expected to detect more, smaller fires than MODIS or AVHRR using compatible detection algorithms. An illustration of the impact of the reduced VIIRS pixel size on expected detection performance is shown in Figure 1. This is an empirical example to provide both simultaneous high-resolution fire information and corresponding MODIS and VIIRS detections at compatible view angle conditions. As we have not been able to generate such configuration with real VIIRS and MODIS data, this example is based on simulated VIIRS radiances, using coincident Advanced Spaceborne Thermal Emission and Reflection Radiometer (ASTER) and MODIS measurements.

For this analysis, first, a fire mask for the 30 m ASTER pixels was created using an ASTER fire detection algorithm [*Giglio et al*., 2008]. Using the ASTER-based fractional fire area estimates, average fire temperature within the MODIS pixel footprint was retrieved by an iterative forward radiative transfer calculation to match calculated radiances with the actual top-of-atmosphere MODIS measurements. The retrieved fire temperature and ASTER-based fire area information were then used to simulate spectral radiances over the grid of the VIIRS pixel footprints [*Schroeder et al*., 2010]. Finally, a hybrid thresholding-contextual detection algorithm was used to generate MODIS and VIIRS detections over the area of the particular ASTER scene. The results shown in Figure 1 indicate not only the better spatial detail of the simulated VIIRS fire maps but also show smaller fires detected by VIIRS and omitted by MODIS.

Additional VIIRS bands providing radiometric signal of hot targets are "imagery" band I4 (3.55–3.93 μm) and the DNB and other shortwave VIIRS bands at night. While these bands are currently not used on the standard VIIRS fire product, their potential use is being explored. Further details on the use of I band data, including caveats, are described in section 6.

Figure 2 shows the results of theoretical simulations of detection limits at 90% probability for nadir view in a boreal ecosystem for MODIS and the VIIRS M band, derived using the methodology described in *Giglio et al*.

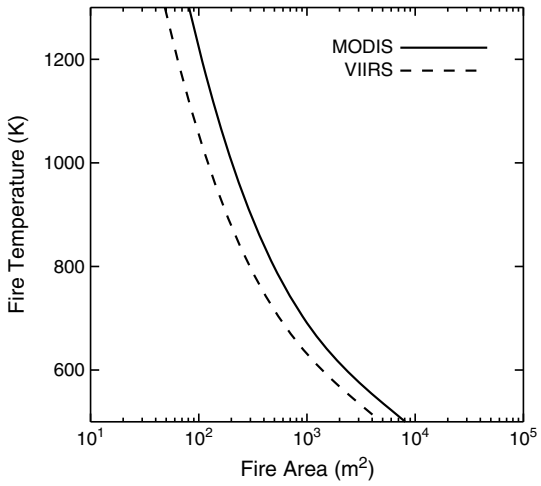

Figure 2. Theoretical detection envelopes for MODIS and VIIRS M band for nadir view and boreal forest vegetation cover. The curves represent fire area and temperature characteristics with a 90% probability of detection.

[1999]. The comparison of the results shows that a fire of a given temperature needs to be larger to be detected by MODIS than by VIIRS, or alternatively, VIIRS should detect a cooler fire of the same size than is applicable for MODIS.

3. The IDPS Active Fires Product

The baseline algorithm for the VIIRS "Active Fires" Application Related Product, which uses primarily the M13 and M15 bands described above, separates fire pixels from nonfire background by a hybrid thresholding-contextual algorithm used to generate the MODIS *Fire and Thermal Anomalies* product. The current operational VIIRS algorithm, executed by Interface Data Processing Segment (IDPS) since VIIRS sensor activation, is the Collection 4 MODIS algorithm equivalent [*Giglio et al*., 2003], applied to spectrally similar VIIRS bands. Correspondence between MODIS and VIIRS bands is shown in *Justice et al*. [2011b], according to which the primary MODIS fire bands 21 and 22 map into VIIRS band M13 and the secondary MODIS fire band 31 maps into VIIRS band M15. No sensor-specific tuning was performed for this initial implementation of the IDPS VIIRS fire detection algorithm. The resulting operational S-NPP VIIRS product delivered by the IDPS consists of a sparse array list of pixels flagged as "fire" by the detection algorithm. A full fire mask and FRP retrievals that are part of the standard MODIS active fire product [*Justice et al*., 2002] are currently not delivered by the IDPS product.

Details of the algorithm are described in the corresponding JPSS Algorithm Theoretical Basis Document (ATBD) [*Joint Polar Satellite System* (*JPSS*), 2013a] and Operational Algorithm Description Document [*JPSS*, 2013b]. A summary of the algorithm elements is provided in Table 1.

4. IDPS Product Evaluation and Validation

The JPSS program has pursued a coordinated Algorithm Development and Calibration/Validation program to ensure and improve the quality of the operational IDPS product. During the early orbit checkout (EOC) and intensive calibration and validation (ICV) periods the focus was on removing processing and algorithmic shortcomings, providing diagnostic feedback to the VIIRS sensor data record (SDR) team based on product discrepancies and initial evaluation of Level 2 product performance. Initial product evaluation of the VIIRS active fire product was done via comparisons with the near-simultaneous Aqua MODIS product. The MODIS fire product is assumed to be validated, based primarily on the extensive validation of the Terra MODIS product using coincident ASTER imagery [*Morisette et al*., 2005; *Csiszar et al*., 2006; *Schroeder et al*., 2008; *Giglio et al*., 2008] and therefore serves as a reliable basis for product consistency check. The ~1:30 h and ~13:30 h local orbital overpass times of the S-NPP and Aqua satellites are similar, and the near-simultaneous observations make direct comparison feasible. This comparison, however, does not constitute a direct validation due to differences in algorithms, sensor characteristics, observing conditions, and the exact timing of the observations.

4.1. Visual Analysis and Comparison of Individual VIIRS and MODIS Scenes

Visual analysis provided initial, first-order evaluation of the S-NPP VIIRS fire product. VIIRS fire imagery, starting with first light imagery available immediately after the opening of the sensor's cryoradiator door on 19 January 2012, showed fire detections consistent with near-coincident Aqua MODIS data (http://earthobservatory.nasa.gov/IOTD/view.php?id=77025). During the EOC and ICV phases of the S-NPP algorithm development and validation program, a number of near-coincident S-NPP VIIRS and Aqua MODIS granules from various locations were processed for direct comparison. Spatial patterns of fire locations from the two sensors were compared by visual inspection. Additionally, VIIRS fire counts within $2° \times 2°$ boxes were calculated and tested for consistency against paired MODIS fire data. In general, the observed fire counts reflected the expected pattern based on relative view angle conditions and corresponding pixel sizes. Note that in addition to often contrasting viewing geometries, algorithm differences and natural

Table 1. Main Elements of the VIIRS IDPS Fire Detection Algorithm, Based on the Algorithm Description Table in the ATBD [*JPSS*, 2013a][a]

Algorithm Component	Description
Identify potential fire pixels	a. Prescreen pixels that have a valid SDR value over land and are classified as "clear" by an internal cloud mask, defined as $(\rho_5+\rho_7)>0.9$ or $T_{16}<265$ K or $\{(\rho_5+\rho_7)>0.7$ and $T_{16}<285$ K$\}$ b. Select potential pixels based on the following criteria i. Daytime: $T_{13}>310$ K and $\Delta T>10$ K and $\rho_7<0.30$ ii. Nighttime: $T_{13}>305$ K and $\Delta T>10$ K
Generate contextual statistics	a. Conduct search in geometric neighborhood of potential fire pixel, ranging from 3×3 pixel box (centered at the potential fire pixel) to 21×21 pixels. i. For each valid clear land pixel in the geometric neighborhood 1. Determine if the pixel is a background fire pixel: a. Daytime: $T_{13}>325$ K and $\Delta T>20$ K b. Nighttime: $T_{13}>310$ K and $\Delta T>10$ K 2. Other clear land pixels are flagged as valid background pixels 3. Accumulate valid background pixel data for statistics on T_{13}, T_{15}, and ΔT ii. Compute: 1. N_t = number of nonfill pixels in neighborhood search 2. N_b = number of valid background pixels in neighborhood search 3. $F_b=N_b/N_t$; fraction valid background pixels iii. If $\{F_b\geq25\%$ and $N_b\geq8\}$ then exit neighborhood search loop; otherwise, search over next larger region b. If the neighborhood search is unsuccessful, flag pixel as unknown and continue with next pixel for fire test; else proceed to next step c. Compute aggregate statistics over selected search region: i. Means for valid background pixels (T_{13B} ,T_{15B}, and ΔT_B) ii. Mean absolute deviations for valid background pixels (δT_{13B}, δT_{15B}, and $\delta\Delta T_B$) iii. Mean absolute deviations for background fires (T'_{13B} and $\delta T'_{13B}$)
Perform absolute fire test	a. Daytime: $T_{13}>360$ K (Test 1; daytime) b. Nighttime: $T_{13}>320$ K (Test 1; nighttime)
Perform contextual fire tests	a. $\Delta T>\Delta T_B+3.5\ \delta\Delta T_B$ (Test 2) b. $\Delta T>\Delta T_B+6$ K (Test 3) c. $T_{13}>T_{13B}+3\ \delta T_{13B}$ (Test 4) d. $T_{15}>T_{15B}+\delta T_{15}-4$ K (Test 5; daytime only) e. $\delta'\ T_{13B}>5$ K (Test 6; daytime only)
Identify fire pixels	a. Daytime: Test 1 or {Test 2 and Test 3 and Test 4 and {Test 5 or Test 6}} are true b. Nighttime: Test 1 or {Test 2 and Test 3 and Test 4} are true
Reject detected fires	a. Sunglint: $\Theta_g<2$ or $\{\Theta_g<8$ and $\rho_5>0.1$ and $\rho_7>0.2$ and $\rho_{11}>0.12\}$ or $\{\Theta_g<12$ and $(N_{aw}+N_w)\}>0$ b. Coast: Define water pixels as $\rho_{11}<0.05$ and $\rho_7<0.15$ and NDVI <0. Reject fires if the number of unmasked water pixels $N_{uw}>0$ and absolute fire test is false. c. Excessive rejection of legitimate background pixels based on the following criteria: $F_b>0.9$ and $N_b>3$ and $T'_{13B}<345$ K and $\delta T'_{13B}<3$ and $\rho_7>0.15$ and $T_{13}<(T'_{13B}+6\ T'_{13B})$

[a] T_{13}, T_{15}, and T_{16} are the VIIRS M13, M15, and M16 brightness temperatures, respectively; $\Delta T=T_{13}-T_{15}$; ρ_i is the VIIRS reflectance in band I; T_{13B}, T_{15B}, and ΔT_B are means for valid background pixels; δT_{13B}, δT_{15B}, and $\delta\Delta T_B$ are mean absolute deviations for valid background pixels; T'_{13B} and $\delta T'_{13B}$ are mean absolute deviations for background fires; Θ_g is the glint angle; N_w is the number of water pixels in search box; and N_{aw} is the number of water pixels within 8 pixels of candidate fire pixel. NDVI is calculated internally as $(\rho_7-\rho_5)/(\rho_7+\rho_5)$. The spectral ranges for the VIIRS bands listed are as follows: M5 [0.662–0.682 μm], M7 [0.846–0.885 μm], M11 [2.225–2.275 μm], M13 [3.973–4.128 μm], M15 [10.263–11.263 μm], and M16 [11.538–12.488 μm].

variations of fires between the VIIRS and MODIS observations make the quantitative interpretation of differences between individual granules complex.

Figure 3 shows an example of the comparison of fire pixels from the VIIRS and Aqua MODIS sensors in the Western United States on 23 August 2012. The larger fires in California observed in the images include the Fort Complex, Bagley, North Pass, Chips, and Rush wildfires. In Oregon, the Waterfalls 2 wildfire can be seen near the top left portion of the images. To the east, in Idaho, the Trinity Ridge and Halstead wildfires can easily be seen. In this example the Aqua MODIS observations had a near-nadir view angle, while the region was near the edge of the VIIRS swath. Despite the suboptimal, off-nadir view angles for VIIRS, the similarities between the detections from the two sensors are remarkable, and the blurriness of the image at the edge of the swath typical for AVHRR or MODIS is minimal on the VIIRS background image. This illustrates the superior spatial sampling features of the VIIRS sensor described above, including the limited degradation of detection performance. Nevertheless, near-nadir Aqua MODIS fire counts were still higher than off-nadir VIIRS counts in California, while in Idaho, which was observed by a more favorable view angle by VIIRS, VIIRS counts outnumbered MODIS. Additional examples of the comparisons can be found at http://viirsfire.geog.umd.edu/, including a range of relative viewing angle configurations.

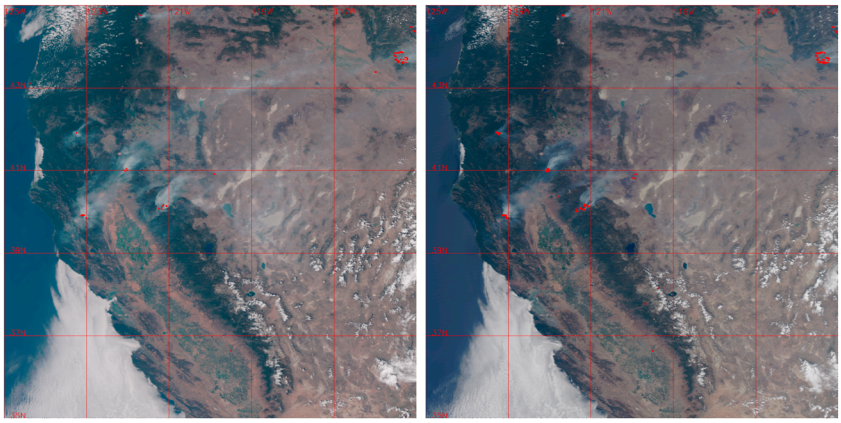

Figure 3. Active fires in the Western United States on 23 August 2012 detected by S-NPP VIIRS (left, 20:10 UTC) and Aqua MODIS (right, 21:05 UTC).

Routine visual analysis, combined with the monitoring of fire counts by VIIRS granule, revealed spurious detections along entire scan lines over clear land, approximately once a day on a global basis during the first 10 months of on-orbit data (Figure 4, left). Causes for such spurious detections were found primarily due to anomalous SDR data (e.g., spurious brightness temperature data in the M13 channel) and the improper handling of bad SDR data by the IDPS fire code (e.g., inconsistent quality flag data). A significant improvement in VIIRS data quality and suitability for statistical comparison occurred when a fix in the SDR code to correct for the dual-gain switching sequence anomaly [see *Cao et al*., 2013b] was implemented in IDPS Mx6.3 on 15 October 2012. The impact of the SDR code correction is illustrated in Figure 4 (right), where the times of data anomalies (*Y* axis) are plotted as a function of day of the year (DOY) (*X* axis). During the first week following the implementation of Mx6.3 on 15 October 2012 (DOY 289), no granules with bad scan lines were detected. Subsequent data quality monitoring showed that the frequency of data anomalies dropped to approximately once a month.

4.2. VIIRS-MODIS Comparative Statistical Analysis

Statistical comparison of fire counts over longer time periods was done as a function of sensor scan angle. A major initial finding from this analysis was the discovery of anomalously low VIIRS fire counts as compared to expectations from prelaunch estimates of relative VIIRS and MODIS detection performance. Figure 5 (left) shows a comparison of VIIRS and Aqua MODIS fire counts as a function of scan angle during the first month of on-orbit VIIRS data. The approximately identical fire counts from the two sensors near nadir (i.e., within the 3 pixel VIIRS aggregation zone) could not be explained solely by algorithm differences, given the considerable differences in pixel sizes. The VIIRS SDR team identified the incorrect pixel aggregation methodology (performed in the brightness temperature space instead of radiance space) as the root cause of the problem. We estimated and later empirically confirmed that this error would typically cause a low bias of approximately 50 K in VIIRS M13 brightness temperatures for average fire pixels, resulting in degraded VIIRS detection

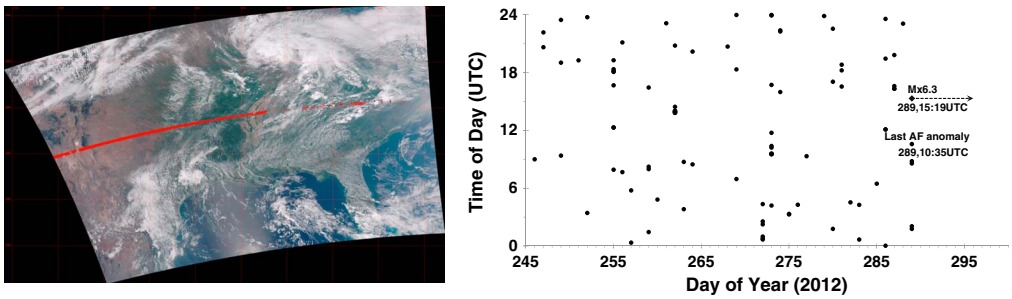

Figure 4. (left) Spurious fire detections due to VIIRS data anomalies on 1 May 2012 at 19:05:29–19:11:09 UTC. (right) Approximate times of data anomalies with spurious detections (*Y* axis) within days of the year (*X* axis) between 2 September and 22 October 2012. Data anomalies occurred approximately once a day until a fix was implemented in IDPS Mx6.3 on 15 October.

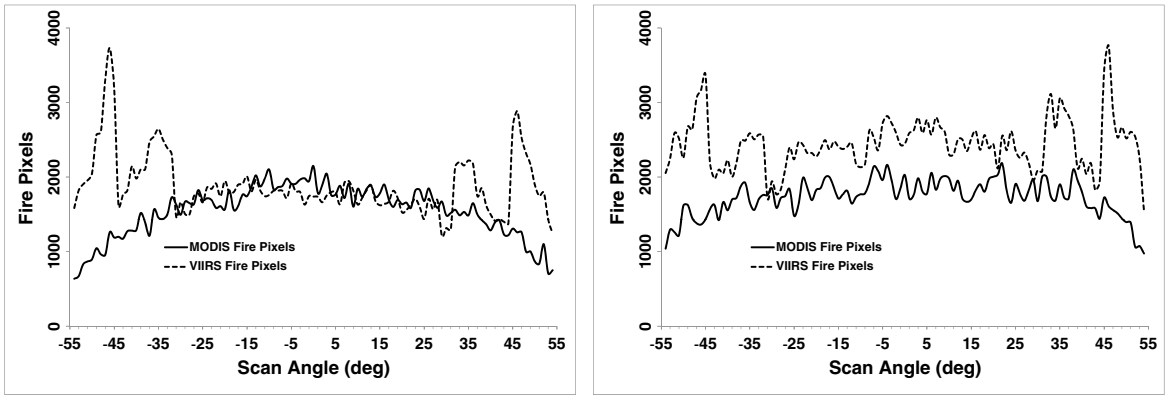

Figure 5. S-NPP/VIIRS and Aqua/MODIS fire pixel detection frequency as a function of scan angle for the period of (left) 19 January to 13 February 2012 and for (right) 11 May to 10 June 2012.

performance through the omission of small and low intensity fires. The VIIRS SDR team developed a code fix, which was implemented in operations with IDPS build Mx5.3 on 3 April 2012. Our analysis of 1 month of global data following this confirmed that the code change indeed resulted in the expected differences between VIIRS fire counts in near-nadir conditions (Figure 5, right).

This comparison was also repeated over 4 months of global data between 15 February and 15 June 2013, amounting to nearly one million VIIRS and over half a million MODIS fire pixels. The overall pattern of the relative fire counts was consistent with that shown in Figure 5 (right). In the 3 pixel VIIRS aggregation zone VIIRS produces approximately 26% more detections than MODIS. In the two- and single-pixel aggregation zones VIIRS produces 70% more detections than MODIS. The higher ratio in this off-nadir scan angle zone is due to the more limited increase of VIIRS pixel size with scan angle compared to MODIS.

Figure 5 also illustrates the relationship between pixel sampling characteristics and detection performance. The bell-shaped curve of the MODIS fire counts reflects the continuous increase of pixel size and the corresponding decrease of detection rates toward high scan angles. In addition to that, prominent bow tie effect is embedded in the MODIS fire pixel statistics artificially inflating the number of off-nadir fire pixels due to oversampling by adjacent scan lines. The onboard processing of VIIRS bow-tie pixels produces fewer fire pixel duplicates compared to MODIS. The curve corresponding to VIIRS counts, however, contains discontinuities at the aggregation switchover angles due to the change of pixel size at those angles.

The implementation date of the M13 aggregation fix in IDPS Mx5.3 was chosen to be the benchmark for the "Beta" maturity status of the active fire product and the public release through NOAA's Comprehensive Large-Array Stewardship System (http://www.class.ncdc.noaa.gov). The Beta release was accompanied by documentation that describes product fundamentals and caveats.

4.3. Toward Explicit Product Validation Using Independent Reference Data

The goal of the VIIRS product validation effort is to follow the approach first developed for the Terra satellite, where MODIS fire products were validated using simultaneous ASTER imagery [*Giglio et al*., 2008] for near-nadir view angles, complemented by a more limited set of near-simultaneous Landsat 5 observations for off-nadir view angles within an acceptable time window of typically less than 15 min [*Csiszar and Schroeder*, 2008]. This approach is driven by the principle that explicit validation of active fire products derived from medium or coarse resolution sensors requires the mapping of the thermal conditions within the entire sensor footprint at a much higher resolution including flaming, smoldering, and nonburning areas [*Morisette et al*., 2005; *Csiszar et al*., 2006; *Schroeder et al*., 2008]. This enables calculation of detection probabilities based on the subpixel fire characteristics determined from the reference data.

For VIIRS, the S-NPP early afternoon orbit prevents use of Landsat-class reference data that are typically acquired in the midmorning hours (~10 h local time). Consequently, the VIIRS fire product validation is building on near-simultaneous high-resolution fire reference data from alternative sources. Airborne observations from sensors such as FireMapper [*Riggan and Hoffman*, 2003], MODIS/ASTER Airborne Simulator [*Hook et al*., 2001], and Autonomous Modular Sensor [*Ambrosia and Hinkley*, 2008] are available through partnerships between

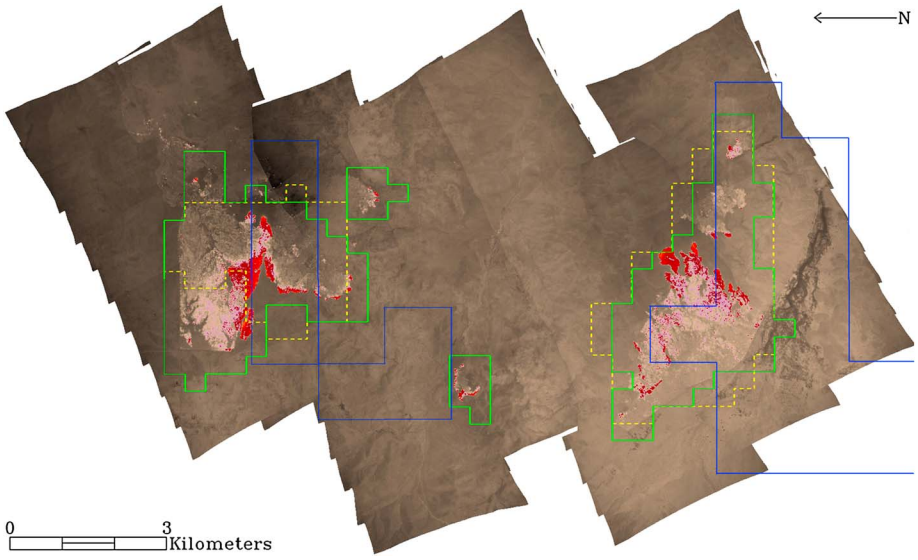

Figure 6. Observations of the Vallecitos fire, CA, on 15 August 2012. The background image was acquired by FireMapper at 21:50 UTC, with the areas of active burning in red. The yellow and green contours show VIIRS detections at 21:00 UTC from M band and I band measurements, respectively. The blue contours show Aqua MODIS detections at 20:15 UTC. The center of the image was observed at 22.1° and 51.8° by VIIRS and MODIS, respectively. The VIIRS and MODIS pixel contours were generated using reprojection tools and represent the approximate nominal footprints.

NOAA, NASA, and the United States Department of Agriculture Forest Service. The airborne imagery provides calibrated data, which not only enable the accurate mapping of fires within the satellite footprint but in case of unsaturated data also allow for the calculation of FRP as validation reference either from midwave infrared measurements or from fire characteristics retrieved from multispectral measurements [e.g., *Matson and Dozier*, 1981; *Riggan et al.*, 2004; *Wooster et al.*, 2003].

Figure 6 shows an example of airborne observations from FireMapper, with VIIRS detections from the M band as well as from the I band (discussed in section 5.2) overlain. For comparison, detections from Aqua MODIS are also shown. The final spatial detail and better mapping accuracy from VIIRS is evident. The MODIS detections appear to be shifted by 1–2 km, particularly in the along-track direction (approximately horizontal on the image). However, in this particular case the area was observed at a lower scan angle (22.1°) by VIIRS than by MODIS (51.8°), and thus, this comparison does not properly reflect the relative detection performance of VIIRS and MODIS. One can also see that the smaller-scale features, such as the fire front near the middle of the image between the two larger complexes, as well as another fire front to the southeast of the large complex in the north, are only detected by VIIRS I band (note that north is to the left on the image). Note also that neither the VIIRS nor the MODIS overpasses were simultaneous with the FireMapper observations. Ensuring observations with all three sensors within a small time window (i.e., up to 30 min) has proven to be logistically difficult.

The limited extent of airborne data constrains a global validation. To increase the spatial extent and sampling of a broader range of fire events across different biomes, international partnerships are also being developed to coordinate coincident observations between S-NPP VIIRS and experimental satellite missions, such as the German Aerospace Center's Technology Experimental Probe (TET-1) and Berlin InfraRed Optical System [*Lorenz*, 2013]. Additionally, these reference data can be used to verify the accuracy of theoretical radiative transfer simulations to estimate the detection capabilities from medium resolution sensors.

Complementing the quantitative validation analyses using airborne reference data, VIIRS fire detection quality assessment is also performed using available ground reports generated by different agencies describing the location and duration of wildland as well as prescribed fire events. Using ground-based information on fires, VIIRS fire detection performance can be assessed for both small and large burns across a wide variety of vegetation types and observation conditions. The sample size of the currently available data is insufficient to derive robust summary statistics.

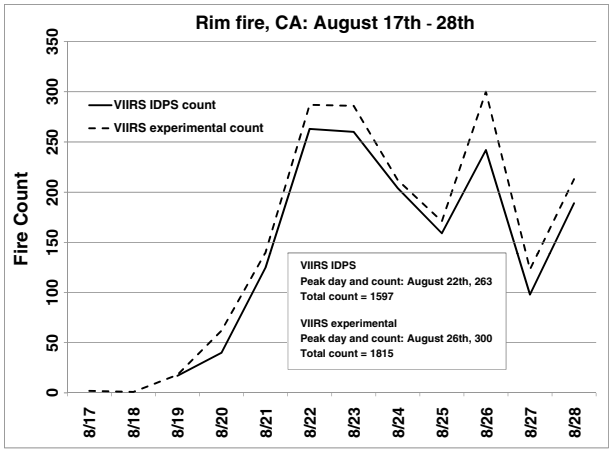

Figure 7. Fire counts from the experimental (dashed line) and IDPS (solid line) VIIRS active fire product over the Rim fire, California, on 17–28 August 2013.

5. VIIRS Active Fire Product Improvements and Enhancements

5.1. Algorithm and Code Development to Ensure Continuity With MODIS

The IDPS VIIRS active fire product currently does not provide continuity with MODIS in terms of processing algorithm or product format and data layers delivered. To address the needs of the user community, an experimental S-NPP VIIRS active fire product has been developed to incorporate algorithm and product format improvements based on the MODIS Collection 6 algorithm. The initial development of the experimental system was undertaken within NASA's Land Product Evaluation and Analysis Tools Element [*Read et al*., 2007] to facilitate the integration of components of the latest MODIS processing code.

The following enhancements of the MODIS Collection 6 algorithm have been implemented: (1) adaptive assignment of potential fire thresholds to better capture small, cool fires and reduce false alarms occurring in hot, arid environments; (2) a new rejection test to eliminate false alarms caused by small clearings within the tropical rainforest regions; (3) extended processing of water pixels to facilitate monitoring of offshore gas flaring; and (4) improvements to the internal cloud mask to eliminate occasional misclassification of snow and desert as cloud. The experimental product also includes FRP retrievals, a spatially explicit fire mask and data layers necessary for generating higher-level products such as the spatially and temporally aggregated climate modeling grid product [*Giglio et al*., 2006]. The experimental product, whose enhancements also served the needs of the NASA Land Science Team [*Justice et al*., 2013b], is available through NASA's Level 1 and Atmosphere Archive and Distribution System (http://ladsweb.nascom.nasa.gov/data/search.html).

Figure 7 shows a comparison of fire counts from the IDPS product and the experimental product over the Rim fire, California, between 17 and 28 August 2013. The experimental product provided 13% more detections (1815) than the IDPS product (1597) for the entire time period.

The JPSS program recently established new Level 1 requirements for the active fire product that include the principal features of the MODIS product (i.e., full fire mask and FRP). The requirements formally apply to the JPSS 1 satellite and beyond. To ensure product readiness by the launch of the JPSS 1 satellite, detailed evaluation and testing is ongoing toward the transition of the updated product into operational production within IDPS. This will include tuning of applicable algorithm coefficients to account for VIIRS sensor characteristics.

While there is a convergence in processing algorithms and product formats, the inherent differences between MODIS-VIIRS sampling geometry and the corresponding differences in the sensitivity to radiative signals from hot spots result in complexities to establish continuity between the MODIS and VIIRS data records. For long-term analysis, however, having compatible capabilities to monitor spatial and temporal patterns of fire dynamics is also useful. As VIIRS tends to detect smaller and cooler fires, the shape of the statistical distribution of fire characteristics may impact the compatibility of trends and patterns from the two sensors. We are fortunate to

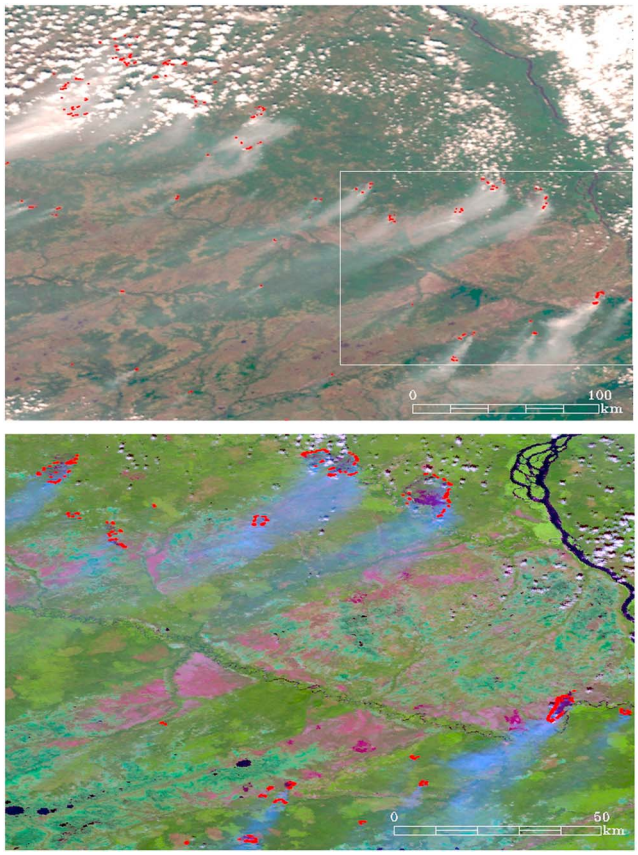

Figure 8. VIIRS detections of various fire complexes in Central Siberia on 16 June 2012 at 6:15 UTC. (top) VIIRS M band 5-4-3 over red-green-blue (RGB) image, bounded by 59°N–61°N latitudes and 84°E–90°E longitudes. (bottom) VIIRS I band 3-2-1 RGB image of the area delineated by the white contour in the top image. Fire detections are shown as red overlay from the IDPS M band product and the experimental I band product, respectively.

have a period of overlapping operation between the two instruments to allow trends to be examined and further analysis of fire populations from moderate or high-resolution data to characterize the compatibility between MODIS and VIIRS.

5.2. VIIRS Fire Detection Using I Band Data

The spectral placement of the 375 m "Imager" bands of VIIRS provides a potential for fire detection at a higher spatial resolution. Band I4 (3.55–3.93 μm) provides the primary radiometric signal from hot spots, while band I5 (10.50–12.40 μm) can be used for background characterization. Because of its spectral band placement, I4 is impacted by an approximately threefold increase in the solar reflection component in the radiometric signal compared to M13. While the explicit removal of the solar reflective component, as well as correction for atmospheric effects, could increase the contrast between fire and background pixels [*He and Li*, 2011], our analysis and empirical evidence suggest that the overall impact of solar reflection remains negligible on the use of the I4 band for fire detection. Following the heritage approaches, an experimental fire mask algorithm was developed and used to analyze selected fire events to explore the full potential of this alternative approach. Details of the I band-based algorithm are documented in *Schroeder et al.* [2014].

Figure 8 shows an example of the comparison of fire detections from the baseline IDPS product (based on M band measurements) and the I band fire masks for the same area in Siberia. The additional spatial detail from the I band detections is obvious. Additionally, the I band mask shows detections for locations where the M band algorithm failed to detect fires. This, as well as the example shown in Figure 6, illustrates the potential for detection of smaller fires in an earlier stage of their development from the I band as well as a more accurate

mapping of burning within individual fire complexes. A further online example of the use of the I band product is available at http://www.nasa.gov/mission_pages/NPP/news/west-blazes.html.

While the experimental product shows good performance over selected areas, an important design feature of the I4 band is its low saturation level (~363 K) compared to the M13 band (~634 K). This feature makes the I4 measurements unsuitable for fire characterization with the exception of relatively small fires. As with M15 channel data, mixing of saturated and unsaturated I4 pixels may occur during data aggregation, noting that both I4 and I5 channels are aggregated on board the spacecraft. Additionally, the sensor exhibits anomalous output for radiance levels beyond saturation due to the folding and wrap around of the radiance counts. This is a behavior consistent with heritage sensors with low saturation, such as AVHRR [*Setzer and Verstraete*, 1994]. Unless this sensor anomaly is eliminated and/or properly flagged, any automated fire detection approach must account for this effect.

6. VIIRS Fire Data to Serve End User Needs

The S-NPP VIIRS active fire development team has been working with selected operational end users on product evaluation, outreach, and data distribution. A product website was set up to provide information on VIIRS fire detection capabilities, products, and sample data access (http://viirsfire.geog.umd.edu). VIIRS fire detections over North America are available through a web-GIS system for the last 2 days. The data are also available in various formats for download through an online archive. Additionally, operational and experimental S-NPP VIIRS products and same-day Terra/Aqua MODIS fire detections are visualized over background true color imagery to facilitate product cross comparisons.

Work is also underway for ensuring low latency data access for the worldwide user community. NASA's Land Atmosphere Near Real-time Capability for EOS (http://earthdata.nasa.gov/data/near-real-time-data/data) and Fire Information and Resource Management System (http://firms.modaps.eosdis.nasa.gov/firemap/) provide a framework for global data distribution that can be adapted to S-NPP data. NOAA's real-time delivery system for S-NPP products through the JPSS Data Exploitation system also provides an additional capability. A further operational data distribution outlet is NOAA's Hazard Mapping System, which includes fire detections from multiple satellites quality controlled by a human analyst.

The VIIRS active fire algorithms are also made available to the user community through the S-NPP Direct Broadcast processing packages. The two major packages supported by NOAA and NASA are the Community Satellite Processing Package (CSPP) University of Wisconsin/Madison (http://cimss.ssec.wisc.edu/cspp/) and the International Polar Orbiter Processing Package (IPOPP) NASA Direct Readout Laboratory (http://directreadout.sci.gsfc.nasa.gov/). The algorithm development team is working on ensuring that the latest algorithm improvements are implemented and documented in both CSPP and IPOPP.

Specific user readiness activities include collaboration with the U.S. domestic fire management community to facilitate the uptake of the VIIRS fire product in operations. The JPSS active fire team has also been working with the NOAA National Weather Service Incident Meteorologists deployed as part of an interagency management team to evaluate and enhance the usefulness of the VIIRS active fire product. As part of this work, progression reports and progression maps are analyzed along with VIIRS active fire data that can provide better spatially explicit mapping of fire activity. This analysis will be augmented by fire intensity information through the use of FRP. Figure 9 shows a comparison of a ground- and air-based fire progression map from the National Interagency Fire Center and the corresponding VIIRS M band detections.

VIIRS fire data will be relevant for fire management in different land use cover types, biomes, and phenological regimes. For this purpose we are engaging regional network scientists from the Global Observation of Forest and Landcover Dynamics (GOFC-GOLD)-Fire program (http://gofc-fire.umd.edu/). GOFC-GOLD-Fire is an international program aimed at refining and articulating the best possible use of fire products from the existing and future satellite observing systems for fire management, policy decision-making, and global change research [*Justice et al*., 2003; *Vadrevu et al*., 2012]. GOFC-GOLD was formed under the Committee on Earth Observation Satellites (CEOS) to bring together data providers and information users to improve access to and use of satellite and ground-based observations on forests and fire [*Csiszar et al*., 2013]. Collaborating with GOFC-GOLD extends the applicability of the current VIIRS active fire research and development internationally. In particular, over a period of years, the GOFC-GOLD program has facilitated the development of

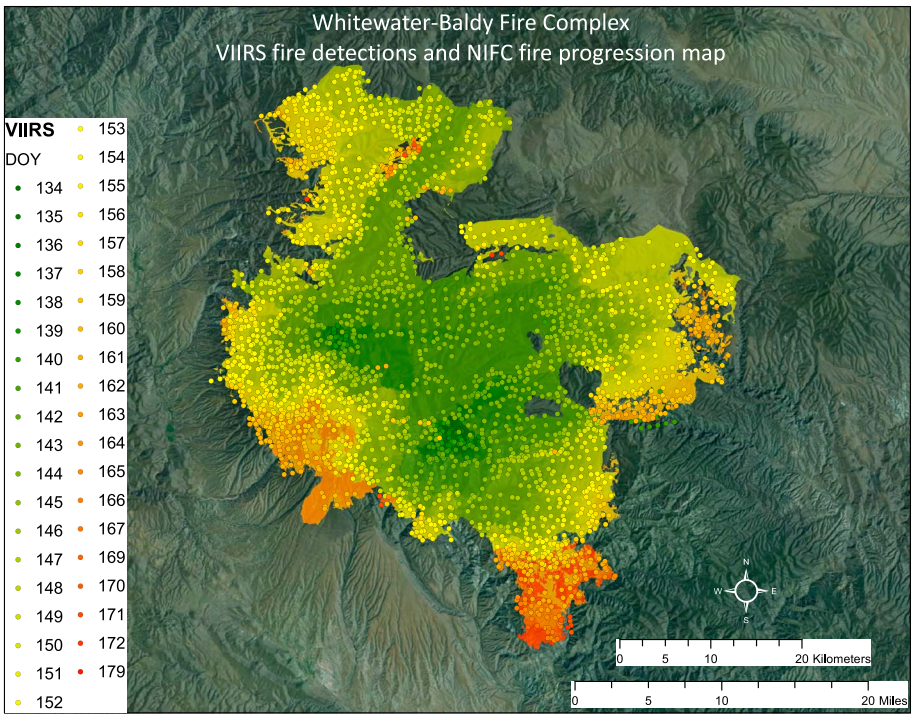

Figure 9. Detected VIIRS M band fire pixels overlaid on a fire progression map of the Whitewater-Baldy fire complex in New Mexico, generated by the National Interagency Fire Center.

several regional networks across the world that act as a forum for lateral exchange of information, data, and expertise within and between regions. A number of regional networks have been established which have an interest in fire monitoring and include the Central Asia Regional Information Network, the Northern Eurasia Regional Information Network, the Miombo Network, Observatoire Satellital des Forêts d'Afrique Centrale, Red Latinoamericana de Teledetección e Incendios Forestales, the Southern African Fire Network, Southeast Asia Regional Research and Information Network, South Eastern European Regional Information Network, West Africa Regional Network, South Central Europe Regional Information Network, Baltic Arctic Regional Information Network, and the South Asia Regional Information Network. The regional networks represent a critical linkage to the regional user community as well as to local experts for product validation and algorithm enhancements. Regional network participants are important users of the Direct Broadcast processing packages and continue to provide invaluable feedback for further product development.

7. Looking Forward

The S-NPP VIIRS instrument provides a new capability to monitor active fires on a global scale, building on the heritage of the MODIS and AVHRR. As described above, the VIIRS provides improvements over these predecessors in active fire detection. The preliminary algorithm currently running in the IDPS demonstrates the instrument's ability to detect active fires, and a number of refinements have been made based on preliminary sensor and data evaluations. Favorable comparisons have been made with MODIS Aqua, airborne, and ground-based fire observations providing the basis for a CEOS Level 1 Validation. Development is now underway to tune and apply the improved algorithm developed for MODIS Collection 6 to VIIRS. At the same time we are working with both domestic and international users of satellite fire data to evaluate the new data and to start to entrain them into their decision-support systems for fire management. VIIRS direct readout capabilities are available, and the VIIRS Fire Team is supporting the associated active fire detection. The team is also working to assess the accuracy of the VIIRS fire detection and characterization, to better understand the relationship to MODIS products, and to characterize the dynamic data continuity. As a system designed to meet operational needs, the VIIRS IDPS does not accommodate data reprocessing. The team therefore stresses the importance of developing the capability to reprocess the VIIRS fire data back to the beginning of

the data record with the new algorithm and with a better understanding of the instrument performance. The team is also encouraging the development of burned area product from VIIRS, the continuity of fire products, and functionality of data delivery systems. With a view to the future and the operational polar orbiters, the team has refined the VIIRS fire detection requirements and is now paying attention to the capability of instruments planned for launch on JPSS 1 and 2 and the constellation of new generation polar fire observations that includes in particular also the Sea and Land Surface Temperature Radiometer on the European Space Agency Sentinel-3 satellite [*Wooster et al*., 2012].

Acknowledgments

This work has been supported by the NOAA JPSS Office, the JPSS Proving Ground and Risk Reduction Program, and the NASA Earth Science Program through the Suomi NPP Science Team for Climate Data Records initiative. We thank Alain Sei and his colleagues at Northrop Grumman Space Technology for the prelaunch development of the VIIRS fire code, Ted Kennelly and his colleagues at Atmospheric Environmental Research, Inc. for prelaunch VIIRS fire capability analysis, and the Raytheon Company for the implementation and maintenance of the operational active fire code in IDPS. We also thank Philip Riggan and the USDA Pacific Southwest Research Station for providing the FireMapper reference data set used in this study, and the three anonymous reviewers for their thorough and constructive reviews. The contents are solely the opinions of the authors and do not constitute a statement of policy, decision, or position on behalf of NOAA or the U.S. Government.

References

Ambrosia, V. G., and E. Hinkley (2008), NASA science serving society: Improving capabilities for fire characterization to effect reduction in disaster losses, *Proc. IEEE Geosc. Remote Sens. Symp.*, *4*, 628–631, doi:10.1109/IGARSS.2008.4779800.

Cao, C., et al. (2013a), Visible Infrared Imaging Radiometer Suite (VIIRS) Sensor Data Record (SDR) User's Guide. Version 1.2, 10 September 2013, NOAA Technical Report NESDIS 142, Available at https://cs.star.nesdis.noaa.gov/NCC/UsersGuideVIIRS.

Cao, C., J. Xiong, S. Blonski, Q. Liu, S. Uprety, X. Shao, Y. Bai, and F. Weng (2013b), NPP VIIRS on-orbit verification, validation, and long-term monitoring, *J. Geophys. Res. Atmos.*, *118*, 11,664–11,678, doi:10.1002/2013JD020418.

Csiszar, I., and W. Schroeder (2008), Short-term observations of the temporal development of active fires from consecutive same-day ETM + and ASTER imagery in the Amazon: Implications for active fire product validation, *IEEE J. Sel. Top. Appl. Earth Obs. Remote Sens.*, *1*, 248–253, doi:10.1109/JSTARS.2008.2011377.

Csiszar, I., J. Morisette, and L. Giglio (2006), Validation of active fire detection from moderate-resolution satellite sensors: The MODIS example in Northern Eurasia, *IEEE Trans. Geosci. Remote Sens.*, 1757–1764, doi:10.1109/TGRS.2006.875941.

Csiszar, I. A., et al. (2013), The GOFC/GOLD Fire Mapping and Monitoring theme: Assessment and strategic plans, in *Remote Sensing Modeling and Applications to Wildland Fires*, edited by J. J. Qu et al., 341–372, Springer and Tsinghua University Press, Heidelberg, Dordrecht, London, New York and Beijing, ISBN: 978-3-642-32529-8.

Dozier, J. (1981), A method for satellite identification of surface temperature fields of subpixel resolution, *Remote Sens. Environ.*, *11*, 221–229.

Elvidge, C. D., I. Nelson, V. R. Hobson, J. Safran, and K. E. Baugh (2001), Detection of fires at night using DMSP-OLS data, in *Global and Regional Fire Monitoring From Space: Planning a Coordinated International Effort*, edited by F. Ahern, J. Goldammer, and C. O. Justice, pp. 125–144, SPB Academic, The Hague, The Netherlands.

Elvidge, C. D., M. Zhizhin, F.-C. Hsu, and K. E. Baugh (2013), VIIRS nightfire: Satellite pyrometry at night, *Remote Sens.*, *5*, 4423–4449, doi:10.3390/RS5094423.

Giglio, L., and C. O. Justice (2003), Effect of wavelength selection on characterization of fire size and temperature, *Int. J. Remote Sens.*, *17*, 3515–3520, doi:10.1080/0143116031000117056.

Giglio, L., and J. D. Kendall (2001), Application of the Dozier retrieval to wildfire characterization—A sensitivity analysis, *Remote Sens. Environ.*, *77*, 34–39, doi:10.1016/S0034-4257(01)00192-4.

Giglio, L., J. D. Kendall, and C. O. Justice (1999), Evaluation of global fire detection algorithms using simulated AVHRR infrared data, *Int. J. Remote Sens.*, *20*, 1947–1985.

Giglio, L., J. Descloitres, C. O. Justice, and Y. Kaufman (2003), An enhanced contextual fire detection algorithm for MODIS, *Remote Sens. Environ.*, *87*, 273–282, doi:10.1016/S0034-4257(03)00184-6.

Giglio, L., I. Csiszar, and C. O. Justice (2006), Global distribution and seasonality of active fires as observed with the Terra and Aqua MODIS sensors, *J. Geophys. Res.*, *111*, G02016, doi:10.1029/2005JG000142.

Giglio, L., I. Csiszar, Á. Restás, J. T. Morisette, W. Schroeder, D. Morton, and C. O. Justice (2008), Active fire detection and characterization with the Advanced Spaceborne Thermal Emission and Reflection Radiometer (ASTER), *Remote Sens. Environ.*, *112*, 3055–3063, doi:10.1016/j.rse.2008.03,003.

He, L., and Z. Li (2011), Enhancement of a fire-detection algorithm by eliminating solar contamination effects and atmospheric path radiance: Application to MODIS data, *Int. J. Remote Sens.*, *32*(21), 6273–6293, doi:10.1080/01431161.2010.508057.

Hillger, D., et al. (2013), First-light imagery from Suomi NPP VIIRS, *Bull. Am. Meteorol. Soc.*, *94*, 1019–1029, doi:10.1175/BAMS-D-12-00097.1.

Hook, S. J., J. J. Myers, K. J. Thome, M. Fitzgerald, and A. B. Kahle (2001), The MODIS/ASTER airborne simulator (MASTER)—A new instrument for earth science studies, *Remote Sens. Environ.*, *76*(1), 93–102, doi:10.1016/S0034-4257(00)00195-4.

Ichoku, C. M., R. Kahn, and M. Chin (2012), Satellite contributions to the quantitative characterization of biomass burning for climate modeling, *Atmos. Res.*, *111*, 1–28, doi:10.1016/j.atmosres.2012.03.007.

Ichoku, C., and Y. Kaufman (2005), A method to derive smoke emission rates from MODIS fire radiative energy measurements, *IEEE Trans. Geosci.Remote Sens.*, *43*(11), 2636–2649.

Joint Polar Satellite System (JPSS) (2013a), Joint Polar Satellite System (JPSS) VIIRS active fires: Fire mask Algorithm Theoretical Basis Document (ATDB), 474-00030, released 07/19/2011, Available at http://npp.gsfc.nasa.gov/science/documents.html.

JPSS (2013b), Joint Polar Satellite System (JPSS) Operational Algorithm Description (OAD) Document for VIIRS Active Fires (AF) Application Related Product (ARP) Software, Revision B, 474-00064, released 03/120/2013, [Available at http://npp.gsfc.nasa.gov/science/documents.html.]

Justice, C. O., and C. J. Tucker III (2009), Coarse resolution optical sensors, in *Handbook of Remote Sensing*, edited by T. A. Warner, M. D. Nellis and G. M. Foody, pp. 139–150, SAGE Publications Inc., London, U.K.

Justice, C. O., L. Giglio, D. Roy, L. Boschetti, I. Csiszar, D. Davies, S. Korontzi, W. Schroeder, K. O'Neal, and J. Morisette (2011a), MODIS-Derived Global Fire Products, in *Land Remote Sensing and Global Environmental Change: NASA's Earth Observing System and the Science of ASTER and MODIS*, vol. 11, Series: Remote Sensing and Digital Image Processing, edited by B. Ramachandran, C. O. Justice and M. J. Abrams, pp. 873, Springer Verlag, New York, Dordrecht, Heidelberg, London.

Justice, C. O., E. Vermote, J. Privette, and A. Sei (2011b), The evolution of U.S. moderate resolution optical land remote sensing from AVHRR to VIIRS, in *Land Remote Sensing and Global Environmental Change: NASA's Earth Observing System and the Science of ASTER and MODIS*, Series: Remote Sensing and Digital Image Processing, vol. 11, edited by B. Ramachandran, C. O. Justice, and M. J. Abrams, pp. 873, Springer Verlag.

Justice, C., I. Csiszar, L. Boschetti, S. Korontzi, W. Schroeder, L. Giglio, K. P. Vadrevu, and D. Roy (2013a), Satellite monitoring and inventory of global vegetation fire, in *Vegetation Fires and Global Change: Challenges for Concerted International Action. A White Paper directed to the United Nations and International Organizations. A publication of the Global Fire Monitoring Center (GFMC)*, edited by J. Goldammer, pp. 400, Kessel Publishing House.

Justice, C. O., et al. (2013b), Land products from Suomi NPP VIIRS: Overview and status, *J. Geophys. Res. Atmos.*, *118*, 9753–9765, doi:10.1002/jgrd.50771.
Justice, C. O., L. Giglio, S. Korontzi, J. Owens, J. T. Morisette, D. P. Roy, J. Descloitres, S. Alleaume, F. Petitcolin, and Y. Kaufman (2002), The MODIS fire products, *Remote Sens. Environ.*, *83*, 244–262, doi:10.1016/S0034-4257(02)00076-7.
Justice, C. O., R. Smith, M. Gill, and I. Csiszar (2003), Satellite-based fire monitoring: Current capabilities, future directions and applications in Australia, *Int. J. Wildland Fire*, *102*, 247–258, doi:10.1071/WF03013.
Kaufman, Y. J., C. O. Justice, L. P. Flynn, J. D. Kendall, E. M. Prins, L. Giglio, D. E. Ward, W. P. Menzel, and A. W. Setzer (1998), Potential global fire monitoring from EOS-MODIS, *J. Geophys. Res.*, *103*(D24), 32,215–32,238, doi:10.1029/98JD01644.
Lasaponara, R., V. Cuomo, M. F. Machiatto, and T. Simoniello (2003), A self-adaptive algorithm based on AVHRR multitemporal data analysis for small active fire detection, *Int. J. Remote Sens.*, *24*(8), 1723–1749.
Li, Z., S. Nadon, and J. Cihlar (2000), Satellite-based detection of Canadian boreal forest fire: Development and application of the algorithm, *Int. J. Remote Sens.*, *21*(16), 3057–3069.
Lorenz, E. (2013), Thermal remote sensing with small satellites: BIRD, TET and the next generation BIROS, *Thermal Infrared Remote Sens.*, *17*, 149–176, doi:10.1007/978-94-007-6639-6_8.
Matson, M., and B. Holben (1987), Satellite detection of tropical burning in Brazil, *Int. J. Remote Sens.*, *8*, 509–516.
Matson, M., and J. Dozier (1981), Identification of subresolution high temperature sources using thermal IR sensor, *Photogram. Eng. Remote Sens.*, *47*, 1311–1318.
Morisette, J., L. Giglio, I. Csiszar, and C. Justice (2005), Validation of the MODIS active fire product over Southern Africa with ASTER data, *Int. J. Remote Sens.*, *26*, 4239–4264.
Read, S. M., R. Wolfe, S. Devadiga, G. Ye, A. Isaacman, C. Davidson, and E. J. Masuoka (2007), LAND PEATE VIIRS Science Data Processing Software System Description version 1.2, NASA/GSFC.
Riggan, P. J., R. G. Tissell, R. N. Lockwood, J. A. Brass, J. A. Raposo Pereira, H. S. Miranda, A. C. Miranda, T. Campos, and R. Higgins (2004), Remote measurement of energy and carbon flux from wildfires in Brazil, *Ecol. Appl.*, *14*(3), 855–872, doi:10.1890/02-5162.
Riggan, P. J., and J. W. Hoffman (2003), FireMapper™: A thermal-imaging radiometer for wildfire research and operations, *IEEE Aerospace Conf. Proc.*, *4*, 1843–1854.
Robinson, J. M. (1991), Fire from space: Global evaluation using infrared remote sensing, *Int. J. Remote Sens.*, *12*, 3–24.
Schroeder, W., E. Prins, L. Giglio, I. Csiszar, C. Schmidt, J. T. Morisette, and D. Morton (2008), Validation of GOES and MODIS active fire detection products using ASTER and ETM + data, *Remote Sens. Environ.*, *112*, 2711–2726, doi:10.1016/j.rse.2008.01.005.
Schroeder, W., I. Csiszar, L. Giglio, E. Ellicott, C. C. Schmidt, J. P. Hoffman, and S. Lindstrom (2010), Early characterization of the active fire detection products derived from the next generation NPOESS/VIIRS and GOES-R/ABI instruments, *IEEE Int. Symp. Geosci. Remote Sens. IGARSS*, 2683–2686, doi:10.1109/IGARSS.2010.5650863.
Schroeder, W., P. Oliva, L. Giglio, and I. Csiszar (2014), The new VIIRS 375 m active fire detection data product: Algorithm description and initial assessment, *Remote Sens. Environ.*, doi:10.1016/j.rse.2013.12.008, in press.
Setzer, A. W., and M. M. Verstraete (1994), Fire and glint in AVHRR's channel 3: A possible reason for the non-saturation mystery, *Int. J. Remote Sens.*, *15*, 711–718.
Setzer, A. W., and M. C. Pereira (1991), Amazonia biomass burnings in 1897 and an estimate of their tropospheric emissions, *Ambio*, *20*, 19–22.
Shephard, M. W., and E. J. Kennelly (2003), Effect of band-to-band coregistration on fire property retrievals, *IEEE Trans. Geosci. Remote Sens.*, *41*, 2648–2661, doi:10.1109/TGRS.2003.814912.
Vadrevu, K. P., I. Csiszar, D. Roy, L. Boschetti, L. Giglio, and C. O. Justice (2012), The GOFC-GOLD fire implementation team workshop-satellite remote sensing of fires: Current progress and future prospects, *The Earth Observer*, *24*(2), 31–35.
Wolfe, R., G. Lin, M. Nishihama, K. P. Tewari, J. C. Tilton, and A. R. Isaacman (2013), Suomi NPP VIIRS prelaunch and on-orbit geometric calibration and characterization, *J. Geophys. Res. Atmos.*, *118*, 11,508–11,521, doi:10.1002/jgrd.50873.
Wooster, M. J., B. Zhukov, and D. Oertel (2003), Fire radiative energy for quantitative study of biomass burning: Derivation from the BIRD experimental satellite and comparison to MODIS fire products, *Remote Sens. Environ.*, *86*, 83–107, doi:10.1016/S0034-4257(03)00070-1.
Wooster, M. J., W. Xu, and T. Nightingale (2012), Sentinel-3 SLSTR active fire detection and FRP product: Pre-launch algorithm development and performance evaluation using MODIS and ASTER datasets, *Remote Sens. Environ.*, *120*, 236–254, doi:10.1016/j.rse.2011.09.033.